

## Article

# MoS<sub>2</sub>/MWCNT-COOH-Modified Glassy Carbon Electrode for Nitrite Detection in Water Environment

Shijie Ren <sup>1,2</sup>, Yahui Zhang <sup>1</sup> , Ruimiao Qin <sup>1,2</sup> , Honggang Xu <sup>1</sup>, Minger Ye <sup>3,\*</sup> and Pengcheng Nie <sup>1,\*</sup>

<sup>1</sup> Institute of Information Technology in Agriculture, College of Biosystem Engineering and Food Science, Zhejiang University, Hangzhou 310027, China

<sup>2</sup> Institute of Agricultural Remote Sensing and Information Technology Application, College of Environmental and Resource Science, Zhejiang University, Hangzhou 310027, China

<sup>3</sup> College of Agriculture and Biotechnology, Zhejiang University, Hangzhou 310027, China

\* Correspondence: mingerye1189@163.com (M.Y.); pcn@zju.edu.cn (P.N.)

**Abstract:** Nitrite is harmful to people and animals when it is excessive in an environment. Traditional detection methods are time-consuming and are generally restricted by sensitivity. In this study, a simple and efficient electrochemical sensor made of a glassy carbon electrode (GCE), modified with MoS<sub>2</sub> nanosheets/carboxylic multiwall carbon nanotubes (MoS<sub>2</sub>/MWCNT-COOH), was used to detect nitrite. Cyclic voltammetry (CV) was used for drawing the standard curve of nitrite. The properties of the modified materials were analyzed by X-ray diffraction (XRD), X-ray photoelectron spectroscopy (XPS), scanning electron microscopy (SEM), transmission electron microscopy (TEM), and electrochemical impedance spectroscopy (EIS). The modified electrode presents a great response to nitrite, shows a wide sensing range (10–10,000 μM) and shows a low detection limit (3.6 μM). The characterization of nanomaterials indicates that MoS<sub>2</sub>/MWCNT-COOH has a big surface area (150.3 m<sup>2</sup> g<sup>-1</sup>) and abundant pores (pore volume is 0.7085 cm<sup>3</sup> g<sup>-1</sup>). In addition, the sensor shows high sensitivity (0.35 μA μM<sup>-1</sup> cm<sup>-2</sup>), good reproducibility (RSD is 2.2%), and good stability (the responding current only decreased about 4% after 2 weeks). Therefore, the MoS<sub>2</sub>/MWCNT-COOH-modified electrode is a potential analytical method in nitrite determination.

**Keywords:** electrochemical sensor; MoS<sub>2</sub>; carboxylic multiwall carbon nanotubes (MoS<sub>2</sub>/MWCNT-COOH); glassy carbon electrode (GCE); cyclic voltammetry (CV)



**Citation:** Ren, S.; Zhang, Y.; Qin, R.; Xu, H.; Ye, M.; Nie, P. MoS<sub>2</sub>/MWCNT-COOH-Modified Glassy Carbon Electrode for Nitrite Detection in Water Environment. *Chemosensors* **2022**, *10*, 419. <https://doi.org/10.3390/chemosensors10100419>

Academic Editor: Yige Zhou

Received: 12 September 2022

Accepted: 10 October 2022

Published: 13 October 2022

**Publisher's Note:** MDPI stays neutral with regard to jurisdictional claims in published maps and institutional affiliations.



**Copyright:** © 2022 by the authors. Licensee MDPI, Basel, Switzerland. This article is an open access article distributed under the terms and conditions of the Creative Commons Attribution (CC BY) license (<https://creativecommons.org/licenses/by/4.0/>).

## 1. Introduction

Nitrite (NO<sub>2</sub><sup>-</sup>) has been extensively applied in food additives, food preservatives, the pharmaceutical industry, and agricultural production activities [1]. Moreover, the accumulation of nitrite in some production environments, such as intensive aquaculture, happens frequently. However, a high concentration of nitrite is harmful to humans and animals. Previous studies have shown that nitrite accumulation could irreversibly transform hemoglobin into methemoglobin in blood, which weakens the oxygen transport capacity and leads to respiratory failure [2,3]. Accordingly, it is important to realize the timely and accurate determination of nitrite in the environment. Various analytical techniques were utilized for the detection of nitrite, such as spectrophotometry, chemiluminescence, chromatography, spectrofluorimetry, and electrochemical detection [1,4,5]. Electrochemical detection has received much attention, which contributes to the fast response, simple pretreatment, and high sensitivity [6]. Many novel materials, especially nanomaterials, were used to improve the performance of electrochemical sensors. Kiattisak Promsuwan et al. have reported on a nitrite sensor based on a poly vinyl alcohol/silver microcubics/polyacrylic acid modified screen-printed carbon electrode. The sensor used novel flow injection amperometry measurement, showed high sensitivity (474.14 μA mM<sup>-1</sup> cm<sup>-2</sup>), and showed good recovery (84–102%) in real samples (ham, bacon, fermented pork, and sausage) [7]. Md. A. Rashed et al. verified the nitrite determination efficiency of a glassy

carbon electrode (GCE) modified with a multiwall carbon nanotube (MWCNT), doped polypyrrole/carbon black through linear sweep voltammetry and chronoamperometry. The low detection limits (LODs) of these two methods were 2.3  $\mu\text{M}$  and 3.06  $\mu\text{M}$ , respectively [8].

$\text{MoS}_2$ , one of the representatives of two-dimensional (2D) layered transition metals, attracts much attention in electrode modification because of its big surface area and excellent electro-catalytic activity [9]. However,  $\text{MoS}_2$  usually needs to combine with other conductive materials such as a carbon nanotube (CNT), graphene, and metal nanoparticles because of  $\text{MoS}_2$ 's poor conductivity [10].  $\text{MoS}_2$  and graphene-oxide composites decreased the internal resistance and enhanced the charge transfer on the electrode surface [11]. A GCE modified with  $\text{Au@MoS}_2$ /chitosan showed a wide detection range (0.05–200  $\mu\text{M}$ ) and low LOD (0.03  $\mu\text{M}$ ) in the determination of monosodium glutamate [12]. Kumar et al. reported a reliable electrochemical sensor for the simultaneous detection of dopamine, ascorbic acid, serotonin, and guanine, based on a poly (alanine)/NaOH/ $\text{MoS}_2$ /MWCNTs modified carbon paste electrode, due to the synergistic benefits of hybrid materials.  $\text{MoS}_2$  offered catalytic capability and poly (alanine)/MWCNTs offered conductivity [13].

CNT has played an important role in super capacitor and electrochemical sensors since it was synthesized, which is thanks to its high conductivity, nano tubulous structure, large surface area, and low price. Carboxylic multiwall carbon nanotubes (MWCNT-COOH) and oxidized CNT could form a conducting network for diffusion ions and is easy to hybridize with other composites such as metal oxides, conductive polymer, metal nanoparticles, transition metal dichalcogenides, and metal organic frameworks [14]. Wang et al. synthesized a 3D core-shell CNT/ $\text{MoS}_2$  hybrid that showed a high battery electrode capacity, thanks to the active sites on the hybrid [15]. Mohammad et al. developed a MWCNT/Cu/PANI hybrid nanocomposite electrode to detect nitrate ions; the electrode improved the reaction process of nitrate [16]. Moreover, due to the synergic effects of the nanocomposites, the charge transfer resistance declined significantly [17]. The previous results indicate that MWCNT and  $\text{MoS}_2$  have great potential in the field of electrochemical sensors.

In this work, we introduce an electrochemical detection sensor, which is a GCE modified with simply synthesized  $\text{MoS}_2$ /MWCNT-COOH composites. The sensor is simple, fast, and efficient. X-ray diffraction (XRD), X-ray photoelectron spectroscopy (XPS), scanning electron microscopy (SEM), and transmission electron microscopy (TEM) were used to evaluate the morphological characteristics and chemical composition of the synthesized composites. Cyclic voltammetry (CV), chronoamperometry (i-t), and electrochemical impedance spectroscopy (EIS) were utilized for testing the electrochemical properties of the modified electrode.

## 2. Materials and Methods

### 2.1. Chemicals

MWCNT-COOH and  $\text{MoS}_2$  were purchased from Nanjing Xianfeng nano technology Co., Ltd. (Nanjing, China). Polyvinylpyrrolidone (PVP), potassium ferricyanide ( $\text{K}_3[\text{Fe}(\text{CN})_6]$ ), potassium ferrocyanide trihydrate ( $\text{K}_4[\text{Fe}(\text{CN})_6]$ ), potassium chloride (KCl), disodium hydrogen phosphate ( $\text{Na}_2\text{HPO}_4$ ), sodium dihydrogen phosphate ( $\text{NaH}_2\text{PO}_4$ ), sodium chloride (NaCl), sodium nitrite ( $\text{NaNO}_2$ ), potassium nitrate ( $\text{KNO}_3$ ), sodium sulphate ( $\text{Na}_2\text{SO}_4$ ), potassium chloride (KCl), calcium chloride ( $\text{CaCl}_2$ ), urea, glucose, sodium carbonate ( $\text{Na}_2\text{CO}_3$ ), hydrogen peroxide, and ascorbic acid were used in the experiment, and all the chemicals were analytical grade. The deionized (DI) water was obtained from an ultra-pure water system.

### 2.2. Instruments

The electrochemical experiments were performed on the CHI660E electrochemical workstation (Shanghai Chenhua Instruments Limited, Shanghai, China) with a three-electrode system, including a working electrode (GCE), a reference electrode (saturated calomel electrode (SCE)), and a counter electrode (platinum plate). All the electrodes were purchased from Wuhan GaoShiRuiLian science and technology Co., Ltd. (Wuhan, China).

Other instruments included cold field emission SEM (Hitachi-SU8010, Tokyo, Japan), TEM (Japan Electron JEM-1400Flash, Tokyo, Japan), XRD (Bruker D8 ADVANCE, Karlsruhe, Germany), and XPS (Escalab 250Xi, Thermo Fisher, Waltham, UK).

### 2.3. Preparation of MoS<sub>2</sub>/MWCNT-COOH/GCE and Electrochemical Measurements

MWCNT-COOH, MoS<sub>2</sub>, and PVP were dispersed in DI water (the concentration of each component is 1 mg/mL) by ultrasonication; this process lasted for 1 h. Before modification, the GCE was polished with 0.3 μm and 0.05 μm Al<sub>2</sub>O<sub>3</sub> slurries in turn, then cleaned with DI water, and dried with nitrogen. Then, 7.5 μL of the prepared composite solution was transferred to the surface of the GCE and dried at room temperature. The buffer solution in the experiment was PBS (pH = 6.0, made by 0.1 M NaCl, 0.1 M Na<sub>2</sub>HPO<sub>4</sub>, and 0.1 M NaH<sub>2</sub>PO<sub>4</sub>). CV measurement worked at the scan rate of 50 mV/s and at the potential range between 0.4 V and 1.2 V. Chronoamperometry measurement worked at the scan rate of 50 mV/s and at the potential of 0.8 V.

### 2.4. Real Samples Preparation

Tap water and river water were used as the real samples. The tap water was obtained from a tap water pipe and the river water was obtained from the West Lake in Hangzhou, China. Before measurement, all the water samples were filtered to remove macroscopic inclusion. Then, PBS was used to regulate the pH of samples to pH 6.

## 3. Results and Discussions

### 3.1. Structural and Morphology Characterization of MoS<sub>2</sub>/MWCNT-COOH Hybrid

The crystal structures of MoS<sub>2</sub>, MWCNT-COOH, and MoS<sub>2</sub>/MWCNT-COOH were studied by XRD. The XRD patterns of these nanocomposites are shown in Figure 1A. MoS<sub>2</sub>/MWCNT-COOH nanocomposite has obvious diffraction peaks at 2θ values of 14.38°, 32.67°, 39.53°, and 49.78°, which corresponds to the (002), (100), (103), and (105) reflection planes of MoS<sub>2</sub>, respectively. All of these diffraction peaks were related to the 2H phase of MoS<sub>2</sub> [18]. Additionally, the interplanar crystal spacing of MoS<sub>2</sub> nanosheets at the (002) plane is 0.615 nm which is the same with previous research, demonstrating that the space structure of MoS<sub>2</sub> was not changed by ultrasonication [19]. The broad diffraction peak at 2θ = 25.56° (002) is the feature peak of MWCNT-COOH, indicating the amorphous carbon structure. The diffraction peak of MWCNT-COOH is broader and lower in the MoS<sub>2</sub>/MWCNT-COOH nanocomposite [20,21]. A crystal structure with low diffraction is good for the interaction between electrolyte ions and the electrode [22].

The surface chemical nature and valence state of the as-prepared composites were analyzed by XPS. The full XPS spectrum of MoS<sub>2</sub>/MWCNT-COOH is shown in Figure S1. The picture (Figure 1B–E) shows the narrow scan spectra of MoS<sub>2</sub>/MWCNT-COOH nanocomposites which contained C1s, O1s, Mo3d, and S2p. The intensity peaks at 284.8 eV, 287.3 eV, and 289 eV in the C1s spectrum (Figure 1B) could be assigned to the C-C bond, C=O bond, and COOH group of MWCNT-COOH, respectively [8]. Another intensity peak at 286 eV relates to the bond of C-O-C/S, indicating the existence of interaction in the interface of MoS<sub>2</sub> and MWCNT-COOH [23]. Furthermore, as shown in Figure 1C, two O-related chemical bonds, C-O and C=O, of O1s, which were located at 532.7 eV and 534.9 eV, respectively, results from the oxygenation of the MWCNT [24]. The Mo3d spectra (Figure 1D) shows three characteristic peaks at 228.9 eV, 232.1 eV, and 226 eV, corresponding to Mo 3d<sub>5/2</sub>, Mo 3d<sub>3/2</sub>, and S2s of MoS<sub>2</sub> phase. The XPS spectra for S2p (Figure 1E) shows the S2p<sub>3/2</sub> high-intensity peak at 161.3 eV, which is because of the existence of the S<sup>2-</sup> in MoS<sub>2</sub> [25,26].

The Brunauer–Emmett–Teller (BET) gas sorptometry measurement was used to analyze the surface area and porous nature of MoS<sub>2</sub>/MWCNT-COOH nanocomposites. The nitrogen (N<sub>2</sub>) adsorption–desorption isotherms of the MoS<sub>2</sub>/MWCNT-COOH hybrid are shown in Figure 2A. The isotherms are identified as II type isotherm, with a type H3 hysteresis loop [27]. A hysteresis loop means that under the same relative pressure, the desorption value is larger than adsorption value, which is related to the capillary condensation of pore

channels. It also indicates the existence of mesopores in the nanocomposites, which is in accordance with the Barret–Joyner–Halenda (BJH) adsorption  $dV/dD$  pore volume results (Figure 2B) [28,29]. The BET surface area was calculated as  $150.3 \text{ m}^2 \text{ g}^{-1}$ . The total pore volume of pores was  $0.7085 \text{ cm}^3 \text{ g}^{-1}$ . The large surface area and abundant pores provide sufficient catalytic sites for nitrite.

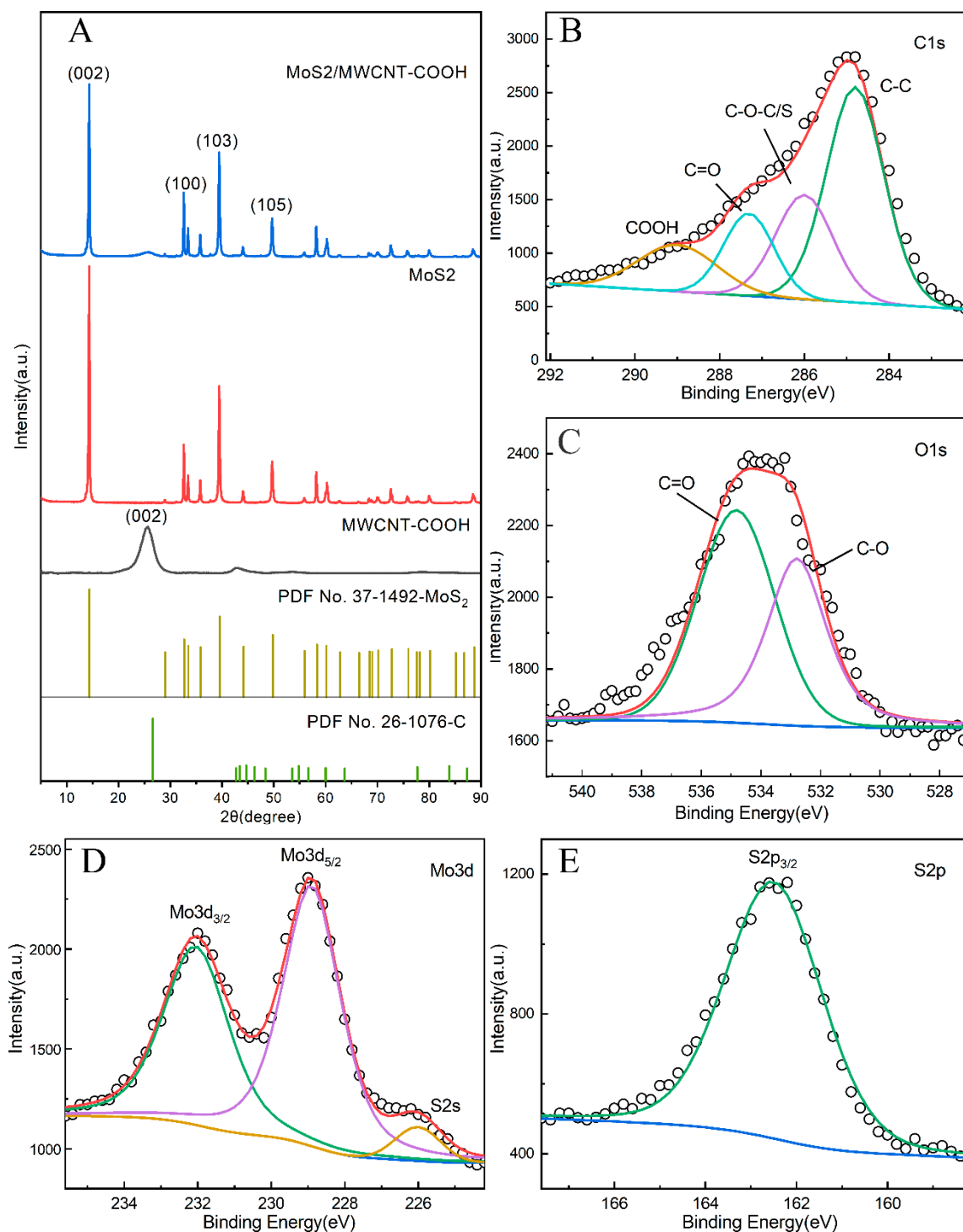


**Figure 1.** XRD spectra (A) of MoS<sub>2</sub>, MWCNT, MoS<sub>2</sub>/MWCNT-COOH, XPS spectra of C1s (B), O1s (C), Mo3d (D), S2p (E).

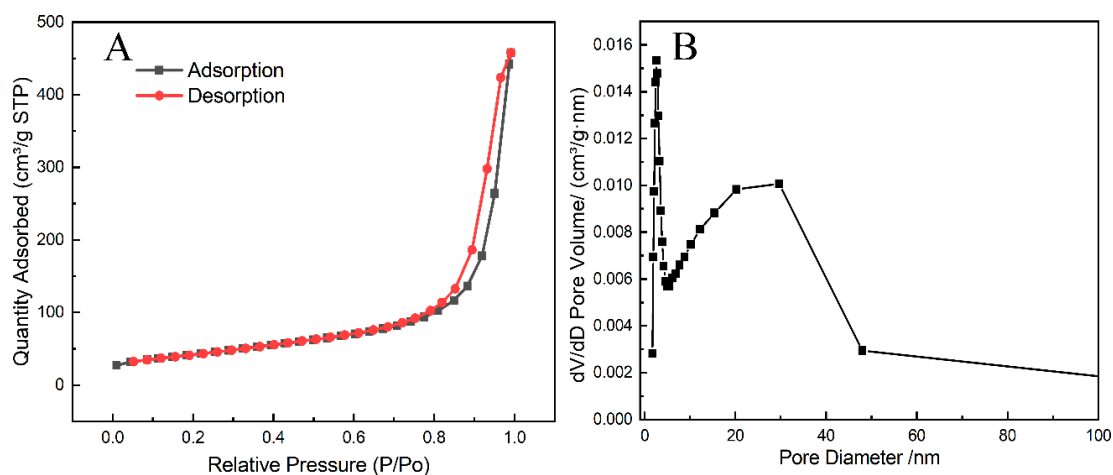


**Figure 2.** Nitrogen ( $N_2$ ) adsorption–desorption isotherms of  $MoS_2$ /MWCNT-COOH hybrid (A), Barret–Joyner–Halenda (BJH) adsorption  $dV/dD$  pore volume of  $MoS_2$ /MWCNT-COOH hybrid (B).

The surface morphology and microstructure of  $MoS_2$ , MWCNT-COOH, and  $MoS_2$ /MWCNT-COOH nanocomposites were characterized by SEM and TEM, and the obtained pictures are shown in Figure 3. The TEM image of MWCNT-COOH (Figure 3A) presents its long tube-like morphology. The multilayer-like structure of  $MoS_2$  is shown in Figure 3B,C. All the traits sufficiently evidence that the prepared materials have large specific surface areas [30,31]. The SEM image (Figure 3D) presents a typical microstructure of a  $MoS_2$ /MWCNT-COOH hybrid; the carbon nanotubes uniformly stick to the  $MoS_2$  nanosheets. It proves the effectiveness of the ultrasonication, which increases the contact area of the composite electrode surface as well as provides a guarantee for the transport of electronic ions [32].

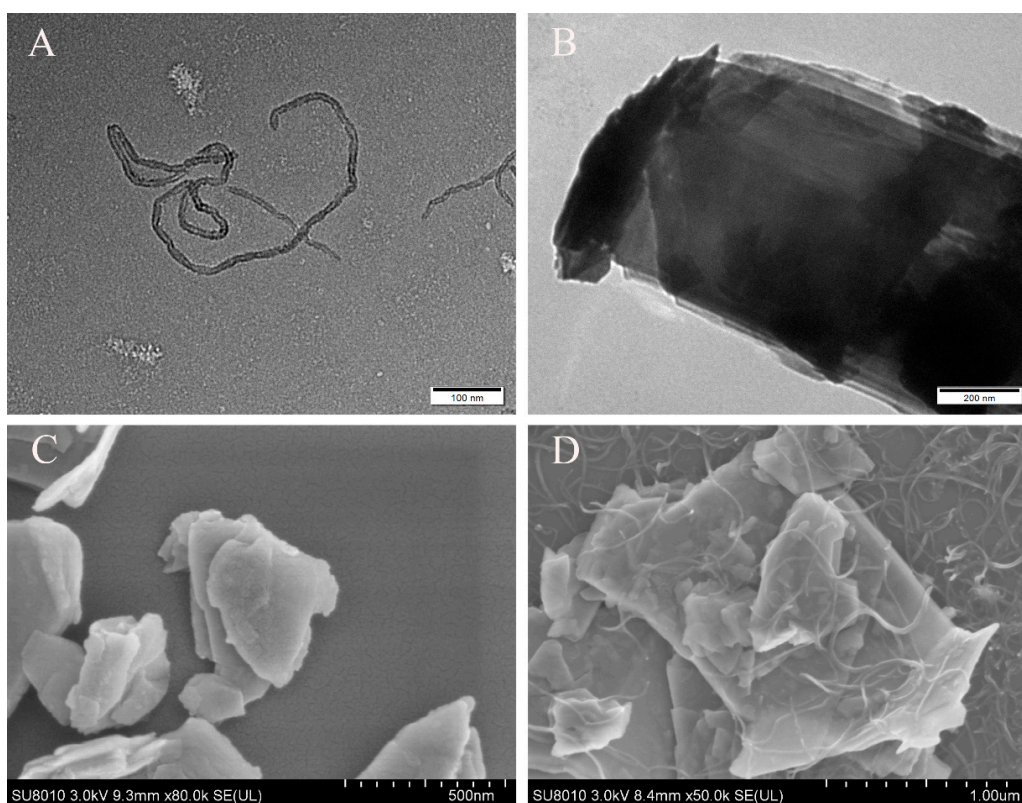


**Figure 3.** TEM images of MWCNT-COOH (A),  $MoS_2$  (B), SEM images of  $MoS_2$  (C),  $MoS_2$ /MWCNT-COOH (D).

### 3.2. Electrochemical Properties of MoS<sub>2</sub>/MWCNT-COOH Hybrid

To evaluate the conductive properties and interfacial features of GCE modified by the as-prepared composites, EIS measurement was operated in 5 mM [Fe(CN)<sub>6</sub>]<sup>3−/4−</sup> solution with a frequency range from 0.01 Hz to 100 kHz. The results are displayed as the Nyquist plots, which are usually composed of a semicircle followed by a straight line. The semicircle at high frequency applies to the electronic transfer restriction process, and the diameter of the semicircle is equal to the electron transfer resistance (Ret) [33]. The straight line at low frequency applies to the diffusion restriction process. As shown in the Figure 4A, MoS<sub>2</sub>/MWCNT-COOH/GCE has the lowest Ret, which means it has better electron-transfer properties than other composites. The poor conductivity of MoS<sub>2</sub> was reconciled by MWCNT-COOH, and the nanosheets structure of MoS<sub>2</sub> improves the surface area of the electrode [34]. Thus, MoS<sub>2</sub>/MWCNT-COOH has superior electronic properties.

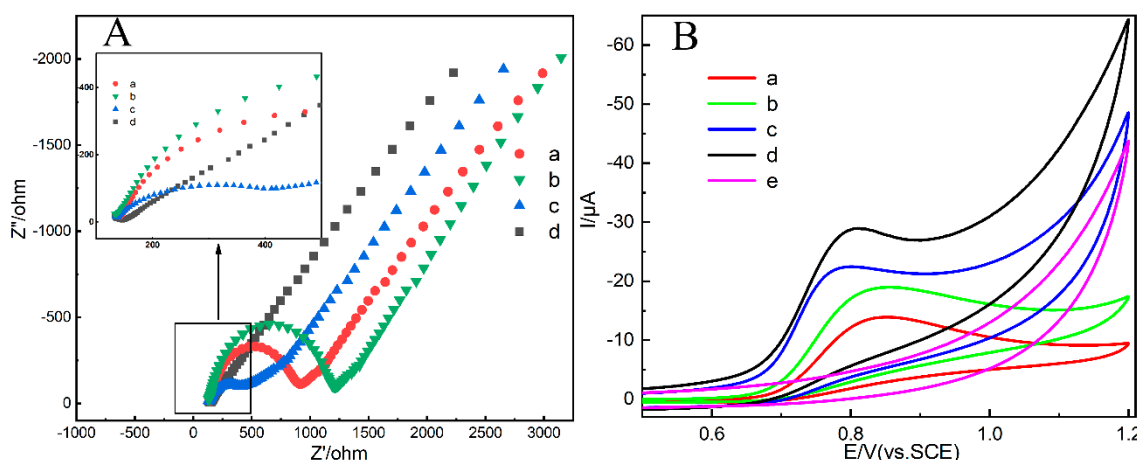


**Figure 4.** Nyquist plots (A) in K<sub>3</sub>[Fe(CN)<sub>6</sub>] solution and CV curves (B) of different modified electrodes: (a) bare GCE, (b) MoS<sub>2</sub>/GCE, (c) MWCNT-COOH/GCE, and (d) MoS<sub>2</sub>/MWCNT-COOH/GCE in 0.1 M PBS with 500 μM nitrite (e) MoS<sub>2</sub>/MWCNT-COOH/GCE in 0.1 M PBS without nitrite.

The CV method was used to compare the catalytic capability of different modified electrodes in phosphate-buffered saline (PBS) with 500 μM NO<sub>2</sub><sup>−</sup>. The CV curves are shown in Figure 4B. The GCE modified with MoS<sub>2</sub>/MWCNT-COOH (Figure 4B(d)) represents a higher peak current value compared to bare GCE (Figure 4B(a)), MoS<sub>2</sub>/GCE (Figure 4B(b)), and MWCNT-COOH/GCE (Figure 4B(c)). Though MoS<sub>2</sub> is generally accepted to have a great catalytic capability, it also has poor conductivity. With the help of MWCNT-COOH's conductivity, MoS<sub>2</sub>/MWCNT-COOH/GCE displays a higher response to NO<sub>2</sub><sup>−</sup> than other comparative electrodes.

### 3.3. Condition Optimization

In order to obtain the best current response of nitrite, different ratios of MWCNT-COOH and MoS<sub>2</sub> (1: 0.25, 0.5, 0.75, 1, 1.25, and 1.5) were studied, respectively, in PBS (pH = 6) with 500 μM NO<sub>2</sub><sup>−</sup> through CV measurements. The results are shown in Figure 5A,B. The highest current appears when the ratio of MWCNT-COOH and MoS<sub>2</sub> is 1:1. In addition, the dispersion time of materials was studied through the same method, and the optimal dispersion time is 60 min (Figure 5C,D).

The different pH of PBS leads to different peak current values of NO<sub>2</sub><sup>−</sup>. Therefore, in order to obtain the best performance, the CV curves of 500 μM NO<sub>2</sub><sup>−</sup> in PBS with different pH values (using the range from 3 to 8) were obtained, and the results are shown in Figure 5E,F. The peak current value at a pH of 6 is shown as the maximum result. Obviously, the PBS of pH value 6 would therefore be the best choice, following the experiments.

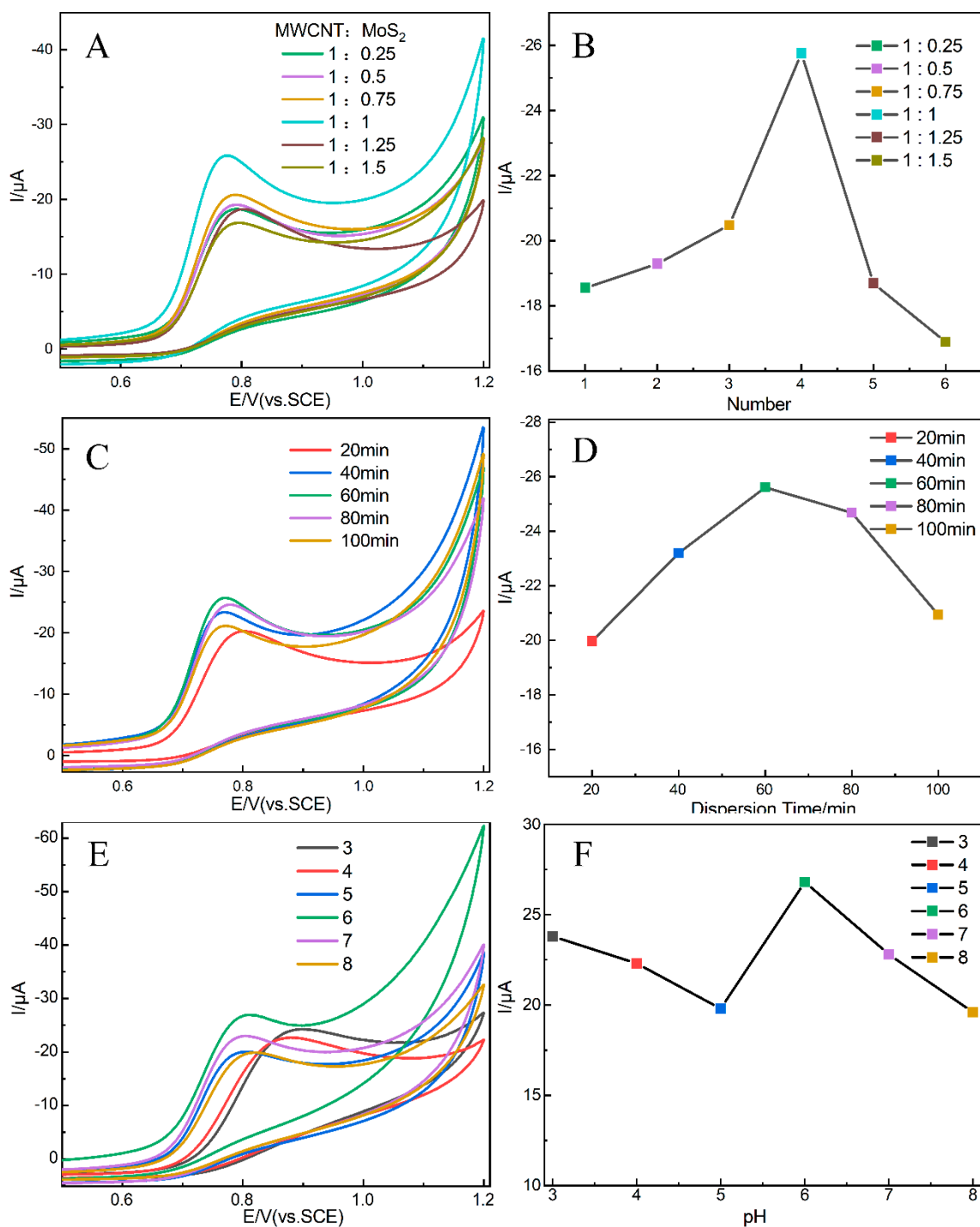


**Figure 5.** CV curves in 0.1 M PBS with 500  $\mu\text{M}$  nitrite and peak current graphs: (A,B) different mix ratios of MWCNT-COOH and MoS<sub>2</sub>, (C,D) different dispersion time of MWCNT-COOH/MoS<sub>2</sub>, (E,F) detection under different pH values.

### 3.4. Scan Rate Analysis and Reaction Mechanism of Nitrite

The analysis of the electrochemical oxidation process of NO<sub>2</sub><sup>-</sup> under different scan rates (25–150 mV/s) was investigated by CV. The CV measurement was operated in PBS (pH = 6) with 500  $\mu\text{M}$  NO<sub>2</sub><sup>-</sup> (Figure 6A). As shown in Figure 6C, the absolute value of the oxidation peak current (*I*) increases linearly with the growth of square root of scan rates ( $v^{1/2}$ ). Meanwhile, the relationship between log *I* and log scan rate (*v*) is linear (Figure 6B), and the regression equation is  $\log I (\log \mu\text{A}) = 0.4747 \log v (\log \text{mV/s}) + 0.6466$ .

The slope is near 0.5. The two results both indicate that a diffusion procedure controls the electrochemical oxidation process of  $\text{NO}_2^-$  [35,36]. It is generally believed that the chemically modified electrode is working by promoting the oxidation–reduction reaction and increasing the adsorption of ions. Although the diffusion process is theoretically a limitation, the modified electrodes still have obvious effectiveness, which implies the electrode modification has exploration significance.

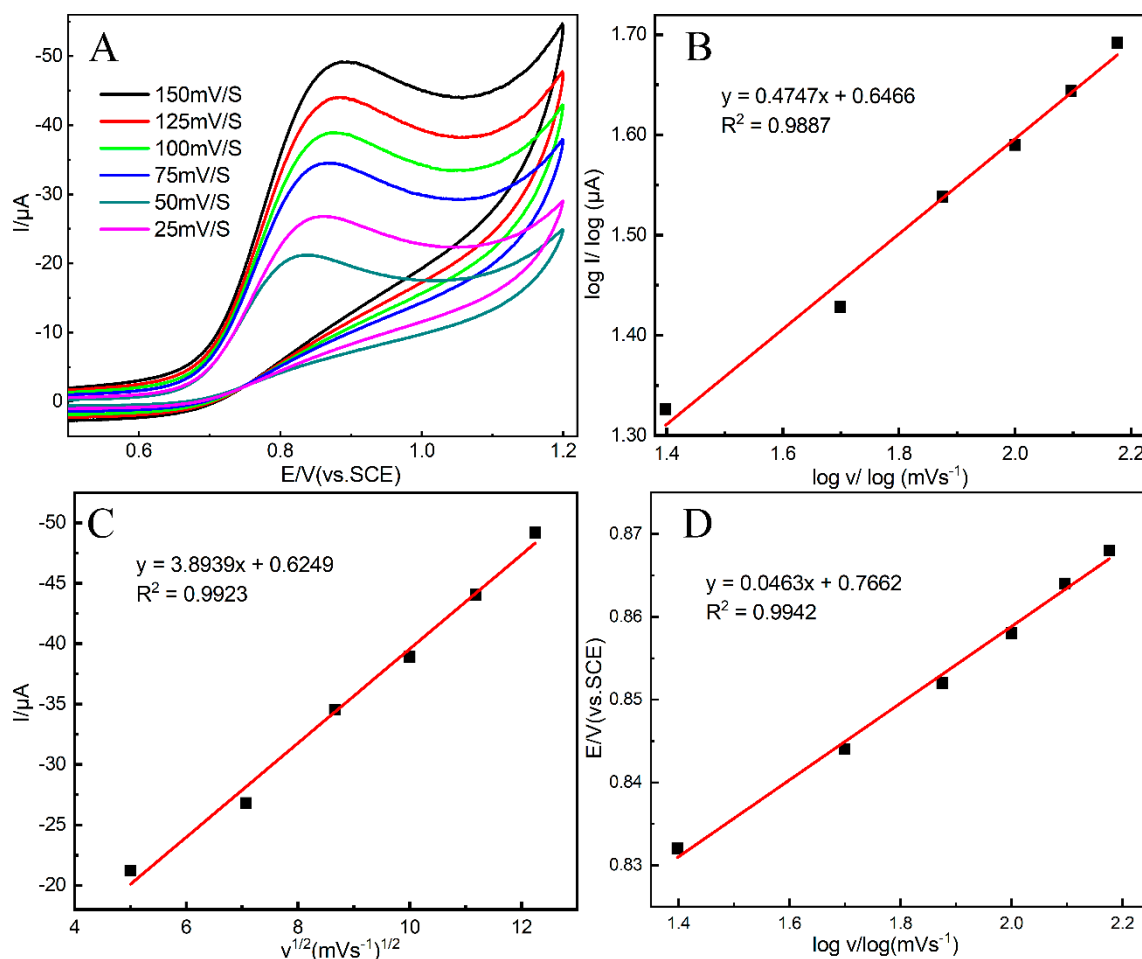


**Figure 6.** (A) CV curves in 0.1 M PBS with 500  $\mu\text{M}$  nitrite under different scan rates, (B) the linear relationship of log current ( $I$ ) and log scan rate ( $v$ ), (C) the linear relationship of log current ( $I$ ) and the square root of scan rate ( $v$ ), and (D) the linear relationship of response potential and log scan rate ( $v$ ).

The anodic peak potential of  $\text{NO}_2^-$  and log scan rate ( $v$ ) has a linear relationship; its linear regression equation of  $E_p$  (V) = 0.0463  $\ln v$  + 0.6843 is shown in Figure 6D. This relationship can be defined by Laviron's theory [37] as shown below:

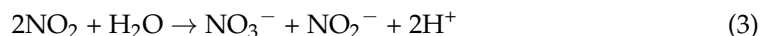
$$E_p = E^0 + (RT/\alpha nF) \ln (RTK^0/\alpha nF) + (RT/\alpha nF) \ln v \quad (1)$$

where  $E^0$  is the formal redox potential (V);  $K^0$  is standard rate constant;  $n$  is the number of transferred electrons in the oxidation–reduction reaction;  $v$  is the scan rate (mV/s);  $\alpha$  is the electron transfer coefficient;  $F$  represents Faraday's constant ( $96,480 \text{ C mol}^{-1}$ ); and  $R$  and  $T$  represent universal gas constant and temperature, respectively. Their convention values are  $8.314 \text{ J mol}^{-1} \text{ K}^{-1}$  and 298 K. Therefore,  $\alpha n$  is calculated as 0.555. According to previous research,  $\alpha$  is estimated at 0.5, usually in an irreversible reaction [38]. Thus, the value of  $n$  is approximate to 1, which indicates that in the oxidation process,  $\text{NO}_2^-$  loses

one electron on the MoS<sub>2</sub>/MWCNT-COOH/GCE. This process can be expressed by the following chemical equation:



Then, NO<sub>2</sub> will be disproportionated to NO<sub>2</sub><sup>-</sup> and NO<sub>3</sub><sup>-</sup>, as shown in the equation under below:



### 3.5. CV Determination of Nitrite

In optimal conditions, the CV measurement was used to detect nitrite under different concentrations by MoS<sub>2</sub>/MWCNT-COOH/GCE. The current responses of nitrite at a range from 10 μM to 10,000 μM are displayed in Figure 7A. It is clear that the CV peak current increases regularly with the increase in nitrite. As shown in Figure 7B, the linear equation is current (I) = -0.0246 concentration (μM) - 13.471, R<sup>2</sup> is 0.9885. It indicates that an electrochemical method based on CV has an accurate response for nitrite detection. According to the fitted equation, the sensitivity of the modified electrode was estimated to be 0.35 μA μM<sup>-1</sup> cm<sup>-2</sup>, which was defined as the ratio of the slope of the linear equation to the surface area of the electrode. The limit of detection (LOD) was 3.6 μM, calculated through the formula 3SD/S (the SD is the standard deviation of a blank signal and the S is the slope of the standard curve). The results prove the new electrochemical sensor is a promising system for nitrite detection.

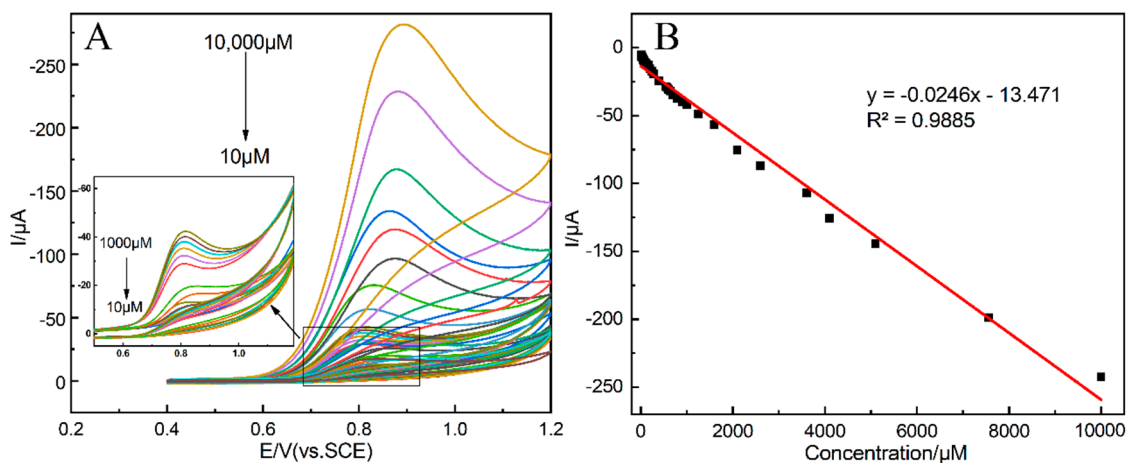


**Figure 7.** (A) CV curves of MoS<sub>2</sub>/MWCNT-COOH/GCE in 0.1 M PBS with nitrite in the range from 10 to 10,000 μM; (B) the fitting equation of the sensor under different concentrations of nitrite.

Table 1 lists the nitrite electrochemical detection parameters of MoS<sub>2</sub>/MWCNT-COOH/GCE, and some other published modified electrodes. It is not difficult to find that MoS<sub>2</sub>/MWCNT-COOH/GCE has a responding performance comparable to that of other nitrite electrochemical sensors and even has better parameters than some of the electrodes in them. MoS<sub>2</sub>/MWCNT-COOH/GCE shows a wider detection range than most of them. The LOD in this research shows a comparable, and even lower than some, value to other sensors. For example, the silver microcubics/poly acrylic acid/poly vinyl alcohol modified screen-printed carbon electrode has the LOD at 4.5 μM [7]; it is 6.75 μM for the laser-induced graphene electrode modified with MWCNT/gold nanoparticles [39]; and it is 16 μM for the α-MnO<sub>2</sub>/MoS<sub>2</sub>/GCE [40]. The comparison table proves that the modified electrode in this work has potential in nitrite determination.

**Table 1.** The comparisons of different modified electrodes on nitrite detection.

Material	Method	Sensitivity ( $\mu\text{A } \mu\text{M}^{-1} \text{ cm}^{-2}$ )	Linear Range	Detection Limit ( $\mu\text{M}$ )	Refs.
Ni/MoS <sub>2</sub> /GCE	DPV <sup>a*</sup>	0.01509	20–1000	2.74	[37]
	i-t	0.00512	5–800	2.48	
Fe <sub>2</sub> O <sub>3</sub> /MoS <sub>2</sub> /GCE	i-t	-	2–6730	1	[41]
AuNPs/MoS <sub>2</sub> /GCE	i-t	0.01239	5–27,800	1.67	[42]
$\alpha$ -MnO <sub>2</sub> -MoS <sub>2</sub> /GCE	i-t	0.516	100–800	16	[40]
MWCNTs/PPy-C/GCE <sup>b*</sup>	LSV <sup>c*</sup>	0.1558	500–10,500	2.3	[8]
	i-t	0.1171	5–9500	3.06	
LIG/MWCNT/AuNPs <sup>d*</sup>	CV	-	10–90	6.75	[39]
Ag/Zr-MOF/FTO <sup>e*</sup>	i-t	-	40–2000	9.1	[43]
AgMCs-PAA/PVA/SPCE <sup>f*</sup>	i-t	0.0596	2–800	4.5	[7]
Au-Dy <sub>2</sub> (WO <sub>4</sub> ) <sub>3</sub> /GCE <sup>g*</sup>	DPV	0.0815	10–1000	3.5	[44]
AgPs-IL-CPE <sup>h*</sup>	SWV	-	50–1000	3	[45]
Poly (4- AB/OT) /CPE <sup>i*</sup>	i-t	0.187	6–600	3.5	[46]
MoS <sub>2</sub> /MWCNT-COOH/GCE	CV	0.35	10–10,000	3.6	This work

<sup>a\*</sup>. Differential Pulse Voltammetry; <sup>b\*</sup>. Multiwall carbon nanotube/polypyrrole-carbon black/GCE; <sup>c\*</sup>. Linear Sweep Voltammetry; <sup>d\*</sup>. Laser-induced graphenous carbon electrode/multiwalled carbon nanotubes/gold nanoparticles; <sup>e\*</sup>. Silver nanoparticles/porphyrinic zirconium-based metal organic framework/fluorine-doped tin oxide (FTO) conducting glass; <sup>f\*</sup>. Silver microcubics-poly (acrylic acid)/poly (vinyl alcohol)/screen-printed carbon electrode; <sup>g\*</sup>. Au nanoparticle-decorated Dy<sub>2</sub>(WO<sub>4</sub>)<sub>3</sub> nanocomposites/GCE; <sup>h\*</sup>. silver sub-micrometre particles/hydrophobic ionic liquid trihexyltetradecylphosphonium chloride/carbon paste electrode; <sup>i\*</sup>. Poly (4-Aminobenzoic Acid/o-Toluidine)-modified carbon paste electrode.

### 3.6. The Selectivity, Reproducibility, and Stability Analysis

The specific selectivity of the suggested electrochemical nitrite sensor was tested by an amperometric method. The obtained i-t curve is shown in Figure 8A. The current has a sudden change after adding nitrite (250  $\mu\text{M}$ , 155 s, 258 s, and 340 s), and when the interfering materials (including KNO<sub>3</sub>, Na<sub>2</sub>SO<sub>4</sub>, KCl, CaCl<sub>2</sub>, urea, glucose, Na<sub>2</sub>CO<sub>3</sub>, hydrogen peroxide, and ascorbic acid) were added, the peak current did not change distinctly. The results of hydrogen peroxide and ascorbic acid are shown in Figure S2. The result proved that the modified electrode has good selectivity on nitrite and confirmed the utilization potential of MoS<sub>2</sub>/MWCNT-COOH nanocomposites in electrochemical materials.

The reproducibility parameter is a key indicator for evaluating the performance of the quantitative analysis. Six MoS<sub>2</sub>/MWCNT-COOH/GCEs under completely identical conditions were used to detect 500  $\mu\text{M}$  of nitrite in PBS (pH = 6), and the peak current of these electrodes are shown in Figure 5B. The differences in the peak current values are very low and the RSD is 2.2%, which verified the reproducibility of the composites.

A good electrode sensor should have good stability. Therefore, three MoS<sub>2</sub>/MWCNT-COOH/GCEs were used to detect 500  $\mu\text{M}$  of nitrite in PBS (pH = 6) every 7 days and they were preserved in a refrigerator after detection. The experiment lasted for 21 days. The average CV curves of each detection day are shown in Figure 8C: the responding current of nitrite on the 7th day and the 14th day decreased by about 4%, and on the 21st day, it decreased by 8.55% (Figure 8D), indicating that the modified electrode has good stability.

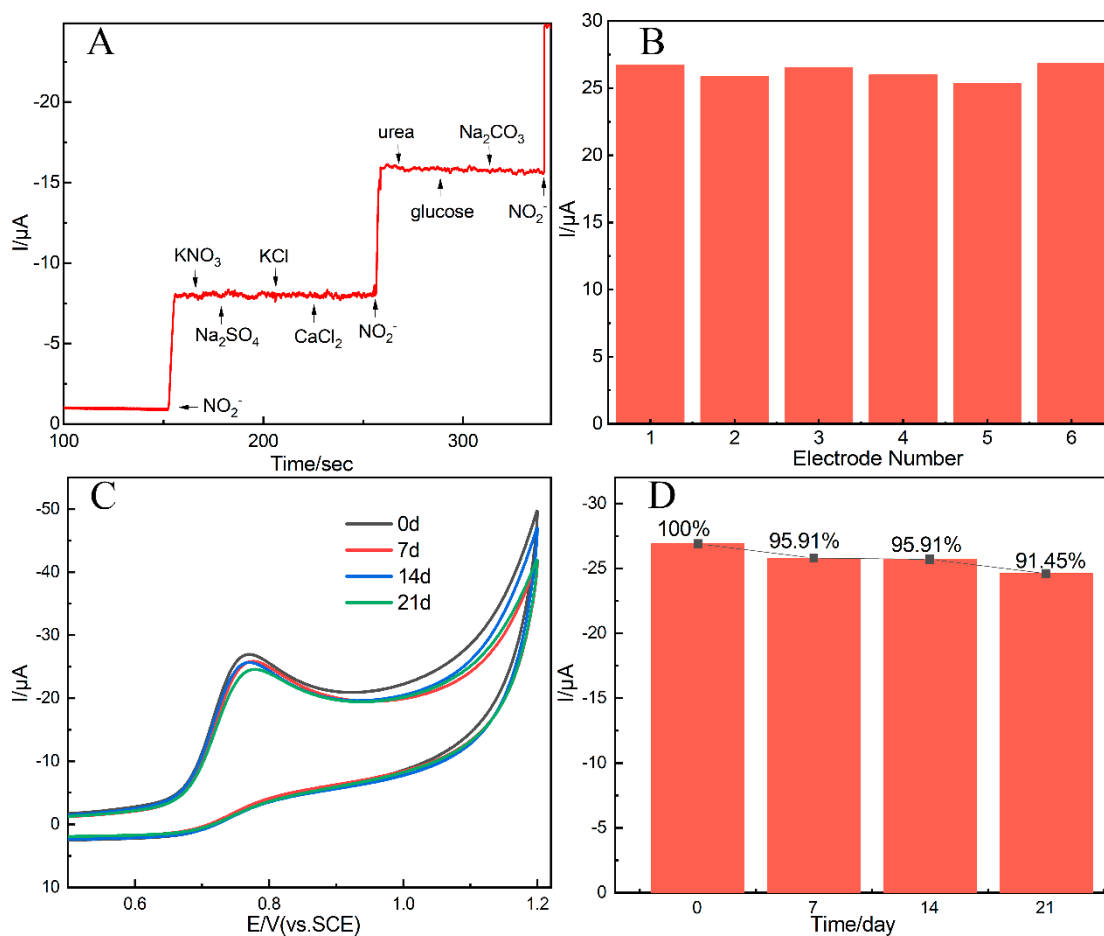


**Figure 8.** (A) The *i*-*t* curves of MoS<sub>2</sub>/MWCNT-COOH/GCE in 0.1 M PBS added with nitrite (250  $\mu\text{M}$ ) and other interfering chemicals (500  $\mu\text{M}$ , respectively), (B) the histograms of six MoS<sub>2</sub>/MWCNT-COOH/GCEs in 0.1 M PBS with 500  $\mu\text{M}$  nitrite, the CV curves (C) and the current histograms (D) of MoS<sub>2</sub>/MWCNT-COOH/GCE in 0.1 M PBS with 500  $\mu\text{M}$  nitrite MoS<sub>2</sub>/MWCNT-COOH/GCE under different preserve time (0 d, 7 d, 14 d, and 21 d).

### 3.7. Real Sample Analysis

The MoS<sub>2</sub>/MWCNT-COOH/GCE successfully detected nitrite in both the tap water and the river water with the standard addition method. Every concentration experiment ran three times, and the average current of three times experiments was used to calculate the nitrite concentration. The real sample verification results are shown in Table 2. The recovery values are between 97.2% and 107%, and RSDs are under 4%. The standard addition calibration curves are shown in Figure S3. The regression function of tap water is  $I (\mu\text{A}) = -0.0267 \text{ concentration } (\mu\text{M}) - 12.603$  ( $R^2 = 0.9525$ ), and the regression function of river water is  $I (\mu\text{A}) = -0.027 \text{ concentration } (\mu\text{M}) - 12.514$  ( $R^2 = 0.9401$ ). The results are close to those of the standard curve method, which also verifies the accuracy of the sensor. Therefore, the sensor has potential to be applied under real environment conditions.

**Table 2.** The determination of real water samples with nitrite added.

Sample	Added ( $\mu\text{M}$ )	Found ( $\mu\text{M}$ )	Recovery (%)	RSD (%) <i>n</i> = 3
Tap water	5	5.23	104.6	2.8
	25	25.32	101.3	2.5
	50	48.60	97.2	3.6
	250	246.25	98.5	1.4
	500	496.50	99.3	0.7
River water	5	5.35	107	2.3
	25	25.50	102	3.1
	50	50.95	101.9	1.9
	250	250.25	100.1	1
	500	497.50	99.5	0.4

#### 4. Conclusions

In this paper, a simple ultrasonication method was used on the synthesis of  $\text{MoS}_2/\text{MWCNT-COOH}$  nanocomposites. The GCE modified by  $\text{MoS}_2/\text{MWCNT-COOH}$ , as the working electrode was used to detect nitrite through the CV method. The electrochemical sensor shows good stability, reproducibility, and selectivity, and at the same time, the sensor has a broad detection range (10–10,000  $\mu\text{M}$ ) and low LOD (3.6  $\mu\text{M}$ ). The great catalysis and response ability of the sensor is mainly due to the conductivity and big surface area of  $\text{MoS}_2/\text{MWCNT-COOH}$  nanocomposites. The real sample analysis indicates that  $\text{MoS}_2/\text{MWCNT-COOH}/\text{GCE}$  has good application potential in nitrite detection.

**Supplementary Materials:** The following supporting information can be downloaded at <https://www.mdpi.com/article/10.3390/chemosensors10100419/s1>, Figure S1: The full XPS spectrum of  $\text{MoS}_2/\text{MWCNT-COOH}$  composites; Figure S2: The i-t curves of  $\text{MoS}_2/\text{MWCNT-COOH}/\text{GCE}$  in 0.1 M PBS added with nitrite (250  $\mu\text{M}$ ) and other interfering chemicals (hydrogen peroxide ( $\text{H}_2\text{O}_2$ ) and ascorbic acid 500  $\mu\text{M}$ , respectively); Figure S3: (A) The standard addition calibration curves of tap water. (B) The standard addition calibration curves of river water.

**Author Contributions:** Conceptualization, S.R.; methodology, S.R.; experiment operation, S.R., Y.Z. and R.Q.; data curation, S.R. and H.X.; writing—original draft preparation, S.R.; writing—review and editing, P.N.; visualization, S.R.; supervision, M.Y. and P.N.; funding acquisition, P.N. All authors have read and agreed to the published version of the manuscript.

**Funding:** This research was funded by Zhejiang Provincial Key R & D plan of China, project number 2021C02025 and 2020C02017.

**Institutional Review Board Statement:** Not applicable.

**Informed Consent Statement:** Not applicable.

**Data Availability Statement:** Not applicable.

**Conflicts of Interest:** The authors declare no conflict of interest.

#### References

- Li, X.; Ping, J.; Ying, Y. Recent Developments in Carbon Nanomaterial-Enabled Electrochemical Sensors for Nitrite Detection. *TrAC Trends Anal. Chem.* **2019**, *113*, 1–12. [CrossRef]
- Stamm, P.; Oelze, M.; Steven, S.; Kröllner-Schön, S.; Kvandova, M.; Kalinovic, S.; Jasztal, A.; Kij, A.; Kuntic, M.; Bayo Jimenez, M.T.; et al. Direct Comparison of Inorganic Nitrite and Nitrate on Vascular Dysfunction and Oxidative Damage in Experimental Arterial Hypertension. *Nitric Oxide* **2021**, *113–114*, 57–69. [CrossRef] [PubMed]
- Xu, S.; Chuang, C.Y.; Malle, E.; Gamon, L.F.; Hawkins, C.L.; Davies, M.J. Influence of Plasma Halide, Pseudohalide and Nitrite Ions on Myeloperoxidase-Mediated Protein and Extracellular Matrix Damage. *Free Radic. Biol. Med.* **2022**, *188*, 162–174. [CrossRef]
- Han, S.; Chen, X. Copper Nanoclusters-Enhanced Chemiluminescence for Folic Acid and Nitrite Detection. *Spectrochim. Acta Part A Mol. Biomol. Spectrosc.* **2019**, *210*, 315–320. [CrossRef]

5. Lin, K.; Xu, J.; Dong, X.; Huo, Y.; Yuan, D.; Lin, H.; Zhang, Y. An Automated Spectrophotometric Method for the Direct Determination of Nitrite and Nitrate in Seawater: Nitrite Removal with Sulfamic Acid before Nitrate Reduction Using the Vanadium Reduction Method. *Microchem. J.* **2020**, *158*, 105272. [[CrossRef](#)]
6. Wang, Q.; Liu, Y.; Campillo-Brocal, J.C.; Jiménez-Quero, A.; Crespo, G.A.; Cuartero, M. Electrochemical Biosensor for Glycine Detection in Biological Fluids. *Biosens. Bioelectron.* **2021**, *182*, 113154. [[CrossRef](#)]
7. Promsuwan, K.; Thavarungkul, P.; Kanatharana, P.; Limbut, W. Flow Injection Amperometric Nitrite Sensor Based on Silver Microcubics-Poly (Acrylic Acid)/Poly (Vinyl Alcohol) Modified Screen Printed Carbon Electrode. *Electrochim. Acta* **2017**, *232*, 357–369. [[CrossRef](#)]
8. Rashed, M.A.; Faisal, M.; Alsaiari, M.; Alsareii, S.A.; Harraz, F.A. MWCNT-Doped Polypyrrole-Carbon Black Modified Glassy Carbon Electrode for Efficient Electrochemical Sensing of Nitrite Ions. *Electrocatalysis* **2021**, *12*, 650–666. [[CrossRef](#)]
9. Coleman, J.N.; Lotya, M.; O'Neill, A.; Bergin, S.D.; King, P.J.; Khan, U.; Young, K.; Gaucher, A.; De, S.; Smith, R.J.; et al. Two-Dimensional Nanosheets Produced by Liquid Exfoliation of Layered Materials. *Science* **2011**, *331*, 568–571. [[CrossRef](#)]
10. Zeng, S.; Hu, S.; Xia, J.; Anderson, T.; Dinh, X.-Q.; Meng, X.-M.; Coquet, P.; Yong, K.-T. Graphene-MoS<sub>2</sub> Hybrid Nanostructures Enhanced Surface Plasmon Resonance Biosensors. *Sens. Actuators B Chem.* **2015**, *207*, 801–810. [[CrossRef](#)]
11. Kiranşan, K.D.; Topçu, E. Free-Standing and Flexible MoS<sub>2</sub>/RGO Paper Electrode for Amperometric Detection of Folic Acid. *Electroanalysis* **2018**, *30*, 810–818. [[CrossRef](#)]
12. Devi, R.; Gogoi, S.; Barua, S.; Sankar Dutta, H.; Bordoloi, M.; Khan, R. Electrochemical Detection of Monosodium Glutamate in Foodstuffs Based on Au@MoS<sub>2</sub>/Chitosan Modified Glassy Carbon Electrode. *Food Chem.* **2019**, *276*, 350–357. [[CrossRef](#)]
13. Kumar, M.; Wang, M.; Kumara Swamy, B.E.; Praveen, M.; Zhao, W. Poly (Alanine)/NaOH/ MoS<sub>2</sub>/MWCNTs Modified Carbon Paste Electrode for Simultaneous Detection of Dopamine, Ascorbic Acid, Serotonin and Guanine. *Colloids Surf. B Biointerfaces* **2020**, *196*, 111299. [[CrossRef](#)] [[PubMed](#)]
14. Sarkar, A.; Chakraborty, A.K.; Bera, S.; Krishnamurthy, S. Novel Hydrothermal Synthesis of CoS<sub>2</sub>/MWCNT Nanohybrid Electrode for Supercapacitor: A Systematic Investigation on the Influence of MWCNT. *J. Phys. Chem. C* **2018**, *122*, 18237–18246. [[CrossRef](#)]
15. Wang, Y.; Ma, Z.; Chen, Y.; Zou, M.; Yousaf, M.; Yang, Y.; Yang, L.; Cao, A.; Han, R.P.S. Controlled Synthesis of Core-Shell Carbon@MoS<sub>2</sub> Nanotube Sponges as High-Performance Battery Electrodes. *Adv. Mater.* **2016**, *28*, 10175–10181. [[CrossRef](#)] [[PubMed](#)]
16. Motaghedifard, M.H.; Pourmortazavi, S.M.; Alibolandi, M.; Mirsadeghi, S. Au-Modified Organic/Inorganic MWCNT/Cu/PANI Hybrid Nanocomposite Electrode for Electrochemical Determination of Nitrate Ions. *Microchim. Acta* **2021**, *188*, 99. [[CrossRef](#)]
17. Chakraborty, I.; Chakrabarty, N.; Senapati, A.; Chakraborty, A.K. CuO@NiO/Polyaniline/MWCNT Nanocomposite as High-Performance Electrode for Supercapacitor. *J. Phys. Chem. C* **2018**, *122*, 27180–27190. [[CrossRef](#)]
18. Qin, J.; Huang, F.; Li, X.; Deng, L.; Kang, T.; Markov, A.; Yue, F.; Chen, Y.; Wen, X.; Liu, S.; et al. Enhanced Second Harmonic Generation from Ferroelectric HfO<sub>2</sub>-Based Hybrid Metasurfaces. *ACS Nano* **2019**, *13*, 1213–1222. [[CrossRef](#)] [[PubMed](#)]
19. Geng, S.; Tian, F.; Li, M.; Liu, Y.; Sheng, J.; Yang, W.; Yu, Y.; Hou, Y. Activating Interfacial S Sites of MoS<sub>2</sub> Boosts Hydrogen Evolution Electrocatalysis. *Nano Res.* **2022**, *15*, 1809–1816. [[CrossRef](#)]
20. Yang, W.; Guo, H.; Xue, R.; Zhao, X.; Guan, Q.; Fan, T.; Zhang, L.; Yang, F.; Yang, W. 0.2CNT/NiSex Composite Derived from CNT/MOF-74 as Electrode Material for Electrochemical Capacitor and Electrochemical Sensor. *Microchem. J.* **2021**, *168*, 106519. [[CrossRef](#)]
21. Yang, M.; Guo, H.; Sun, L.; Wu, N.; Wang, M.; Yang, F.; Zhang, T.; Zhang, J.; Pan, Z.; Yang, W. Simultaneous Electrochemical Detection of Hydroquinone and Catechol Using MWCNT-COOH/CTF-1 Composite Modified Electrode. *Colloids Surf. A Physicochem. Eng. Asp.* **2021**, *625*, 126917. [[CrossRef](#)]
22. Karade, S.S.; Dubal, D.P.; Sankapal, B.R. Decoration of Ultrathin MoS<sub>2</sub> Nanoflakes over MWCNTs: Enhanced Supercapacitive Performance through Electrode to Symmetric All-Solid-State Device. *ChemistrySelect* **2017**, *2*, 10405–10412. [[CrossRef](#)]
23. Chen, B.; Lu, H.; Zhou, J.; Ye, C.; Shi, C.; Zhao, N.; Qiao, S.-Z. Porous MoS<sub>2</sub>/Carbon Spheres Anchored on 3D Interconnected Multiwall Carbon Nanotube Networks for Ultrafast Na Storage. *Adv. Energy Mater.* **2018**, *8*, 1702909. [[CrossRef](#)]
24. Prasad, J.; Singh, A.K.; Yadav, A.N.; Kumar, A.; Tomar, M.; Srivastava, A.; Kumar, P.; Gupta, V.; Singh, K. Molybdenum Disulfide-Wrapped Carbon Nanotube-Reduced Graphene Oxide (CNT/MoS<sub>2</sub>-RGO) Nanohybrids for Excellent and Fast Removal of Electromagnetic Interference Pollution. *ACS Appl. Mater. Interfaces* **2020**, *12*, 40828–40837. [[CrossRef](#)] [[PubMed](#)]
25. Di, S.; Ding, P.; Wang, Y.; Wu, Y.; Deng, J.; Jia, L.; Li, Y. Interlayer-Expanded MoS<sub>2</sub> Assemblies for Enhanced Electrochemical Storage of Potassium Ions. *Nano Res.* **2020**, *13*, 225–230. [[CrossRef](#)]
26. Arunbalaji, S.; Vasudevan, R.; Arivanandhan, M.; Alsalmeh, A.; Alghamdi, A.; Jayavel, R. CuO/MoS<sub>2</sub> Nanocomposites for Rapid and High Sensitive Non-Enzymatic Glucose Sensors. *Ceram. Int.* **2020**, *46*, 16879–16885. [[CrossRef](#)]
27. Sing, K.S.W.; Rouquerol, F.; Rouquerol, J. 5-Classical Interpretation of Physisorption Isotherms at the Gas-Solid Interface. In *Adsorption by Powders and Porous Solids*, 2nd ed.; Rouquerol, F., Rouquerol, J., Sing, K.S.W., Llewellyn, P., Maurin, G., Eds.; Academic Press: Oxford, UK, 2014; pp. 159–189. ISBN 978-0-08-097035-6.
28. Ahammad, A.J.S.; Pal, P.R.; Shah, S.S.; Islam, T.; Hasan, M.; Qasem, M.A.A.; Odhikari, N.; Sarker, S.; Kim, D.M.; Aziz, A. Activated Jute Carbon Paste Screen-Printed FTO Electrodes for Nonenzymatic Amperometric Determination of Nitrite. *J. Electroanal. Chem.* **2019**, *832*, 368–379. [[CrossRef](#)]

29. Zhu, X.; Liu, P.; Ge, Y.; Wu, R.; Xue, T.; Sheng, Y.; Ai, S.; Tang, K.; Wen, Y. MoS<sub>2</sub>/MWCNTs Porous Nanohybrid Network with Oxidase-like Characteristic as Electrochemical Nanozyme Sensor Coupled with Machine Learning for Intelligent Analysis of Carbendazim. *J. Electroanal. Chem.* **2020**, *862*, 113940. [[CrossRef](#)]
30. Li, S.; Liu, Y.; Zhao, X.; Cui, K.; Shen, Q.; Li, P.; Qu, X.; Jiao, L. Molecular Engineering on MoS<sub>2</sub> Enables Large Interlayers and Unlocked Basal Planes for High-Performance Aqueous Zn-Ion Storage. *Angew. Chem.* **2021**, *133*, 20448–20455. [[CrossRef](#)]
31. Lu, X.; Liu, G.; Di, P.; Li, Y.; Xue, T.; Duan, X.; Wen, Y.; Zhu, Y.; Cai, Y.; Xu, Q.; et al. Electrochemical Nanozyme Sensor Based on MoS<sub>2</sub>-COOH-MWCNT Nanohybrid for a New Plant Growth Regulator 5-Nitroguaiacol. *Food Anal. Methods* **2020**, *13*, 2028–2038. [[CrossRef](#)]
32. Chen, Y.; Waterhouse, G.I.N.; Qiao, X.; Sun, Y.; Xu, Z. Sensitive Analytical Detection of Nitrite Using an Electrochemical Sensor with STAB-Functionalized Nb<sub>2</sub>C@MWCNTs for Signal Amplification. *Food Chem.* **2022**, *372*, 131356. [[CrossRef](#)] [[PubMed](#)]
33. Retter, U.; Lohse, H. Electrochemical Impedance Spectroscopy. In *Electroanalytical Methods: Guide to Experiments and Applications*; Scholz, F., Bond, A.M., Compton, R.G., Fiedler, D.A., Inzelt, G., Kahlert, H., Komorsky-Lovrić, Š., Lohse, H., Lovrić, M., Marken, F., et al., Eds.; Springer: Berlin/Heidelberg, Germany, 2010; pp. 159–177. ISBN 978-3-642-02915-8.
34. Zhang, Y.; Wang, B.; Lv, S.; Wu, Y.; Jiang, L.; Wang, J.; Liu, X.; Yan, X.; Wang, C.; Sun, P.; et al. Introduction of MWCNT for Enhancing Sensitivity of Room-Temperature Mixed-Potential Type NO Sensor Attached with Ni-MOF Sensing Electrode. *Sens. Actuators B Chem.* **2022**, *361*, 131736. [[CrossRef](#)]
35. Abrego-Martinez, J.C.; Jafari, M.; Chergui, S.; Pavel, C.; Che, D.; Sijaj, M. Aptamer-Based Electrochemical Biosensor for Rapid Detection of SARS-CoV-2: Nanoscale Electrode-Aptamer-SARS-CoV-2 Imaging by Photo-Induced Force Microscopy. *Biosens. Bioelectron.* **2022**, *195*, 113595. [[CrossRef](#)]
36. Tajik, S.; Beitollahi, H.; Ahmadi, S.A.; Askari, M.B.; Di Bartolomeo, A. Screen-Printed Electrode Surface Modification with NiCo<sub>2</sub>O<sub>4</sub>/RGO Nanocomposite for Hydroxylamine Detection. *Nanomaterials* **2021**, *11*, 3208. [[CrossRef](#)]
37. Laviron, E. General Expression of the Linear Potential Sweep Voltammogram in the Case of Diffusionless Electrochemical Systems. *J. Electroanal. Chem. Interfacial Electrochem.* **1979**, *101*, 19–28. [[CrossRef](#)]
38. Yang, Y.; Zhang, J.; Li, Y.W.; Shan, Q.; Wu, W. Ni Nanosheets Evenly Distributed on MoS<sub>2</sub> for Selective Electrochemical Detection of Nitrite. *Colloids Surf. A Physicochem. Eng. Asp.* **2021**, *625*, 126865. [[CrossRef](#)]
39. Nasraoui, S.; Al-Hamry, A.; Anurag, A.; Teixeira, P.R.; Ameer, S.; Paterno, L.G.; Ben Ali, M.; Kanoun, O. Investigation of Laser Induced Graphene Electrodes Modified by MWNT/AuNPs for Detection of Nitrite. In Proceedings of the 2019 16th International Multi-Conference on Systems, Signals & Devices (SSD), Istanbul, Turkey, 21–24 March 2019; Volume 3, pp. 615–620.
40. Sha, R.; Gopalakrishnan, A.; Sreenivasulu, K.V.; Srikanth, V.V.; Badhulika, S. Template-Cum-Catalysis Free Synthesis of  $\alpha$ -MnO<sub>2</sub> Nanorods-Hierarchical MoS<sub>2</sub> Microspheres Composite for Ultra-Sensitive and Selective Determination of Nitrite. *J. Alloy. Compd.* **2019**, *794*, 26–34. [[CrossRef](#)]
41. Wang, H.; Chen, P.; Wen, F.; Zhu, Y.; Zhang, Y. Flower-like Fe<sub>2</sub>O<sub>3</sub>@MoS<sub>2</sub> Nanocomposite Decorated Glassy Carbon Electrode for the Determination of Nitrite. *Sens. Actuators B Chem.* **2015**, *220*, 749–754. [[CrossRef](#)]
42. Zhang, S.; Tang, Y.; Chen, Y.; Zheng, J. Synthesis of Gold Nanoparticles Coated on Flower-like MoS<sub>2</sub> Microsphere and Their Application for Electrochemical Nitrite Sensing. *J. Electroanal. Chem.* **2019**, *839*, 195–201. [[CrossRef](#)]
43. Wang, Y.C.; Chen, Y.C.; Chuang, W.S.; Li, J.H.; Wang, Y.S.; Chuang, C.H.; Chen, C.Y.; Kung, C.-W. Pore-Confined Silver Nanoparticles in a Porphyrinic Metal–Organic Framework for Electrochemical Nitrite Detection. *ACS Appl. Nano Mater.* **2020**, *3*, 9440–9448. [[CrossRef](#)]
44. Zhang, Y.-M.; Huang, H.-P.; Xu, L. A Novel Electrochemical Sensor Based on Au-Dy<sub>2</sub>(WO<sub>4</sub>)<sub>3</sub> Nanocomposites for Simultaneous Determination of Uric Acid and Nitrite. *Chin. J. Anal. Chem.* **2020**, *48*, e20032–e20037. [[CrossRef](#)]
45. Menart, E.; Jovanovski, V.; Hočevar, S.B. Silver Particle-Decorated Carbon Paste Electrode Based on Ionic Liquid for Improved Determination of Nitrite. *Electrochem. Commun.* **2015**, *52*, 45–48. [[CrossRef](#)]
46. Norouzi, B.; Rajabi, M. Fabrication of Poly(4-Aminobenzoic Acid/o-Toluidine) Modified Carbon Paste Electrode and Its Electro-catalytic Property to the Oxidation of Nitrite. *J. Anal. Chem.* **2017**, *72*, 897–903. [[CrossRef](#)]